PCCP

Accepted Manuscript

This is an *Accepted Manuscript*, which has been through the Royal Society of Chemistry peer review process and has been accepted for publication.

Accepted Manuscripts are published online shortly after acceptance, before technical editing, formatting and proof reading. Using this free service, authors can make their results available to the community, in citable form, before we publish the edited article. We will replace this *Accepted Manuscript* with the edited and formatted *Advance Article* as soon as it is available.

You can find more information about *Accepted Manuscripts* in the Information for Authors.

Please note that technical editing may introduce minor changes to the text and/or graphics, which may alter content. The journal's standard Terms & Conditions and the Ethical guidelines still apply. In no event shall the Royal Society of Chemistry be held responsible for any errors or omissions in this *Accepted Manuscript* or any consequences arising from the use of any information it contains.

ROYAL SOCIETY OF CHEMISTRY

www.rsc.org/pccp

PCCP

COMMUNICATION

Observation of Viscoelasticity in Boron Nitride Nanosheet Aerogel

Xiaoliang Zeng,[a,b,†] Lei Ye,[c,†] Rong Sun,[a,*] Jianbin Xu,[c,*] and Ching-Ping Wong[c,d]

Received 00th January 20xx,
Accepted 00th January 20xx

DOI: 10.1039/x0xx00000x

www.rsc.org/

Viscoelasticity of boron nitride nanosheet (BNNS) aerogel has been observed and investigated. It is found that the BNNS aerogel has high damping ratio (0.2), while it exhibits lightweight and negligible temperature dependence below 180 °C. The creep behavior of the BNNS aerogel markedly demonstrats its strain dependence on stress magnitude and temperature, and can be well simulated by the classical models.

Aerogels, composed of interconnected three dimensional (3D) networks, have attracted intensive attention because of their unique properties, such as lightweight,[1, 2] porosity,[3] and high surface area.[4] In recent years, graphene aerogels have sparked widespread interest due to their unique physical and chemical properties.[5-10] Boron nitride nanosheets (BNNSs), an analogue of graphene,[11] also have generated much excitement by their unique properties, including superb corrosion resistance,[12, 13] high thermal conductivity, chemical durability and oxidation resistance.[14-21] The combination of these features makes BNNSs aerogel attractive as a multifunctional and high performance aerogel material. However, studies on the physical and chemical properties of BNNS aerogel were rarely reported.

On the other hand, viscoelasticity, exhibited both viscous and elastic characteristics when a material is exterted to deformation, is one of fascinating physical properties of material.[22, 23] A fundamental understanding of the viscoelastic behaviour is of paramount importance, because it provides the basis for material design in various applications as well as for in-use lifetime analysis in the related technologies.[24] Typical viscoelastic materials are polymers and their composites.[25] Interestingly, it is found that carbon nanotube aerogels also possess unique viscoelasticity.[22, 26, 27] Inspired by the viscoelastic behaviour of carbon nanotube aerogels, we wonder whether BNNS aerogel possesses the similar viscoelasticity or not. Although the compressive properties of the BNNS aerogel were analyzed in previous study,[28] measurement of its viscoelasticity has not been demonstrated. Herein, we have designed and conducted a series of experiments to explore the viscoelasticity of BNNS aerogel, including its dynamic viscoelasticity and creep behaviour under different stress magnitude and at temperature. In addition, the creep behaviour has been simulated by classical models.

To prepare BNNS aerogels, we firstly fabricated noncovalent functionalized BNNSs (NF-BNNSs) via a combination of liquid exfoliation and noncovalent functionalization methods, similar to our previous work (for experimental details, see the ESI).[29] It should be noted that noncovalent functionalization not only effectively prevents the BNNS aggregation, but also improves their chemical activity with polymer.[30] The thickness of the obtained BNNSs varied from few to several layers with a typical size of 200-300 nm, as shown by TEM observation (Figure S1, ESI). The existence of hydroxyl groups and the extent of functionalization (5 wt%) for NF-BNNSs were verified by Fourier transform infrared spectroscopy (FTIR) spectra and thermogravimetric analysis (TGA), respectively, as shown in our previous research.[29] The BNNS aerogels used in here were prepared by frozen-casting method (for experimental details, see the ESI). In a typical procedure, BNNS solution was mixed with cross-linked agent, 1, 4-butanediol diglycidyl ether (BDGE). It was then placed for 4 h at ambient temperature to obtain BNNS hydrogel. After frozen-drying, a BNNS aerogel was produced. Finally, the aerogel was cured at 150 °C for 2 h to improve its mechanical strength. The BDGE content in the aerogel was controlled to be 10, 20, 30 wt%, by adjusting the concentration of the BNNS solution. The corresponding BNNS aerogels were designated as, BNNS aerogel-10, BNNS aerogel-20, and BNNS aerogel-30, respectively. The accurate BDGE content of BNNS aerogel-10, BNNS aerogel-20, and BNNS aerogel-30 was calculated by TGA, to be approximately 9.1, 17.6, and 29.3 wt%, respectively (Figure S2, ESI).

The as-prepared BNNS aerogels had low apparent density of ca. 15-35 mg cm^{-3}, which made it stand stably on the top of a dandelion, as shown in Figure 1a. Figure 1b schematically shows the possible formation mechanism of BNNS aerogels. The BNNSs can connect with each other via cross-linked agent (BDGE), because of the epoxy

[a] Shenzhen Institute of Advanced Technology, Chinese Academy of Sciences, Shenzhen, 518055, China. Email: rong.sun@siat.ac.cn
[b] Shenzhen College of Advanced Technology, University of Chinese Academy of Sciences, Shenzhen, 518055, China.
[c] Department of Electronics Engineering, The Chinese University of Hong Kong, Hong Kong, China. Email: jbxu@ee.cuhk.edu.hk
[d] School of Mechanical Engineering, Georgia Institute of Technology, 771 Ferst Drive, Atlanta, Georgia 30332, United States.
† Xiaoliang Zeng and Lei Ye contributed equally to this work.
Electronic Supplementary Information (ESI) available: [Preparation of BNNS and BNNS aerogel. Characterization of NF-BNNS (TEM and TGA results). Schematic of viscoelastic property calculation procedure. SEM images of cellular structures of BNNS aerogel. The simulated parameters of the generalized Voigt-Kelvin model and Weibull distribution function at different test condition.]. See DOI: 10.1039/x0xx00000x

Physical Chemistry Chemical Physics Accepted Manuscript

Please do not adjust margins

ring-opening reaction between epoxy group of BDGE and hydroxyl attached on the surface of the NF-BNNSs. The porosity of all BNNS aerogels is estimated to be 99% based on calculation using the apparent density and a density of 2.2 g cm^{-3} for BNNS. The high porosity and microstructure are observed by scanning electron microscope (SEM) analysis. As shown in Figure 1c, the aerogel exhibits relatively ordered honeycomb-like cellular structure, with the cell dimension of ~ 100 µm (inset of Figure 1c). Because of its high porosity, the BNNS aerogel can recover completely after compressed, as shown in Figure 1d.

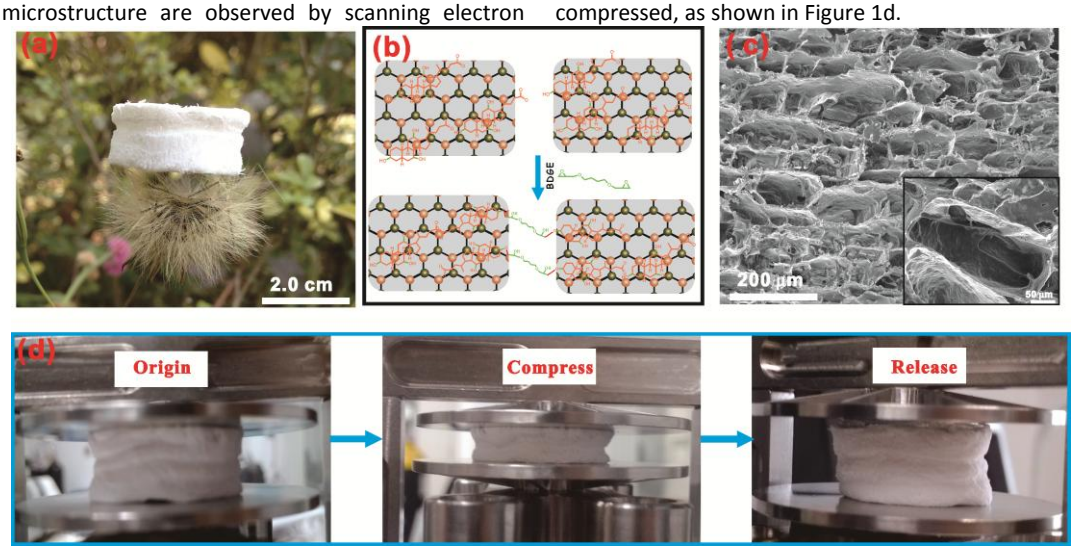

Figure 1. Macro- and microstructure and compressible properties of BNNS aerogel-20. (a) An aerogel with the density of 21 mg cm^3 standing on dandelion. (b) Scheme of the formation mechanism of BNNS aerogel. (c) Typical top-view SEM micrograph of BNNS aerogel. There exist a lot of honeycomb-like cellular structures. The Inset shows a zoom-in SEM image of the aerogel. (d) A set of real-time optical images of a compressed sample showing the recovering process.

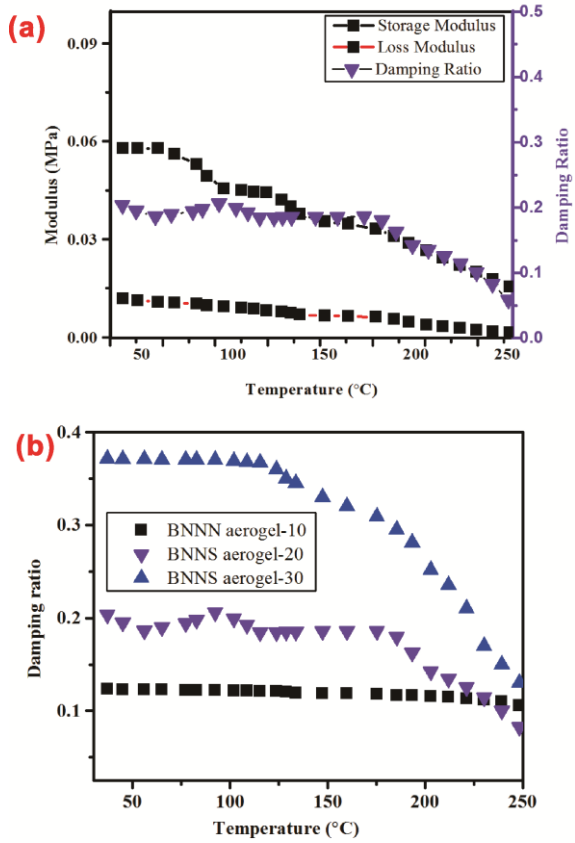

Figure 2. (a) Storage and loss moduluses and damping ratio of BNNS-20 aerogel as a function of temperature. (b) Damping ratio of BNNS aerogel as a function of temperature with different BDGE contents.

The viscoelastic properties were examined using a dynamic mechanical analyzer (DMA, TA, Q800) in compression mode. The tests were carried out in a chamber with flowing N_2 at the rate of 100 mL/min. The dynamic viscoelasticity was tested where a sinusoidal stress was applied to the sample and a resultant sinusoidal strain was measured. The measurements were performed at 1 Hz and at a heating rate of 3 °C /min from 30 to 200 °C. The temperature dependence of the storage modulus (G'), loss modulus (G"), and tangent of phase difference (damping ratio, the ratio of storage modulus to loss modulus) were obtained. As shown in Figure S3 (See the ESI), G' represents the flexural rigidity related to the amount of stored energy, whereas G" represents the amount of dissipated energy in the materials.[31] Figure 2a shows G", G' and damping ratio of BNNS-20 aerogel as a function of temperature. At room temperature, the G' and G" values are 0.058 and 0.012 MPa, respectively, corresponding to the damping ratio of 0.20, which is much higher than that of the pure epoxy resin (0.02), and a little less than that of rubber and CNT-based damping materials (0.3).[25] The high damping ratio means high energy dissipation, which is essential for applications in aerospace, automotive and sports equipment industries. Besides the high damping, another promising advantage in our BNNS aerogel is the lightweight (21 mg cm^{-3}), which is extremely interested by the trend of increasingly light and thin in industry. The BDGE content plays a key role in the damping ratio. Figure 2b shows damping ratio as a function of temperature for BNNS aerogels with different BDGE contents. For BNNS-10 aerogel, low BDGE content results in a low damping ratio (0.12), which limits the application as damping materials. On the other hand, for BNNS-30 aerogel, although it presents higher damping ratio (0.37) at room temperature due to high BDGE content (30 wt%), it shows a high sensitivity to temperature, which is also detrimental as damping materials. Among these three BNNS aerogels, BNNS-20 aerogel displays the best damping properties. The excellent damping behaviour of BNNS

Physical Chemistry Chemical Physics Accepted Manuscript

This journal is © The Royal Society of Chemistry 20xx

Please do not adjust margins

aerogel-20 is partly ascribed to the intrinsic viscoelasticity of epoxy resin (BDGE). However, the pure epoxy material shows a very low damping ratio (0.02), as previous study.[25] The excellent damping behaviour may be mainly assigned to the ordered honeycomb-like cellular structure and the high thermal conductivity of BNNSs. First, it has proved that oriented fillers along a thickness direction of composites leads to high damping ratio.[32] Similarly, its elastic modulus of BNNSs along the out-of-plane direction is much lower than that along a in-plane direction. Correspondingly, the interfacial slip along the out-of-plane direction is rather easily triggered under compressive load , which then results in much higher dissipation of energy. Second, high thermal conductivity of BNNSs may be conducive to release of the generated thermal energy at the interface, leading to the high damping performance. With the temperature increase, G′ gradually decrease, whearas G″ and damping ratio remain unchanged until the temperature up to 180 °C. Above 180 °C, the damping ratio decreases, due to the polymer molecular motion. For the pure rubber[26] and damping composites,[31-34] they showed the pronounced temperature dependence of damping in the range from 25 to 150 °C. This is attributed to temperature dependence of molecular motion in polymer. In our BNNS-20 aerogel, because of the less contribution of polymer to damping, it shows temperature-independent damping ratio below 180 °C.

Creep recovery test is one of the standard experiments to analyze the viscoelasticity. In the test, a constant stress is applied in a preset period and then released, while the strain is monitored as a function of time. In this study, the creep test was performed using stress of 0.005, 0.01, and 0.02 MPa, which was maintained for 10 min, respectively. Figure 3a shows the creep performance of the BNNS aerogel-20 at different constant stress. Under a preset constant stress, the strain creeps and reaches a maximum value. Upon stress release, the aerogel recovers to a certain strain. Different constant stress leads to different deformability, which increases from 7% to 70%, when the constant stress increases from 0.005 to 0.02 MPa. The percentage recovery which is the ability to return from deformation decreases from 100% for 0.005 MPa stress to 23% for 0.02 MPa stress. For 0.005 MPa stress, the induced strain belongs to the Hookean strain. Therefore, the aerogel can fully recover to its original state upon stress release. When the constant stress increases to 0.01 MPa, corresponding to the relatively flat stress plateau, the viscosity of polymer begins to play their roles. After the strain reaches 70%, corresponding to the densification of cells, most of compression is irreversible, as shown in SEM micrographs (Figure S4, ESI). To further characterize the temperature dependence of the creep behaviour, the creep test was conducted at 30, 60, 90, and 180 °C, respectively. As shown in Figure 3b, as the temperature increases from 30 to 180 °C, the deformability increases from 25% to 28%. This may be ascribed to the thermally-activated softening of the polymer matrix.

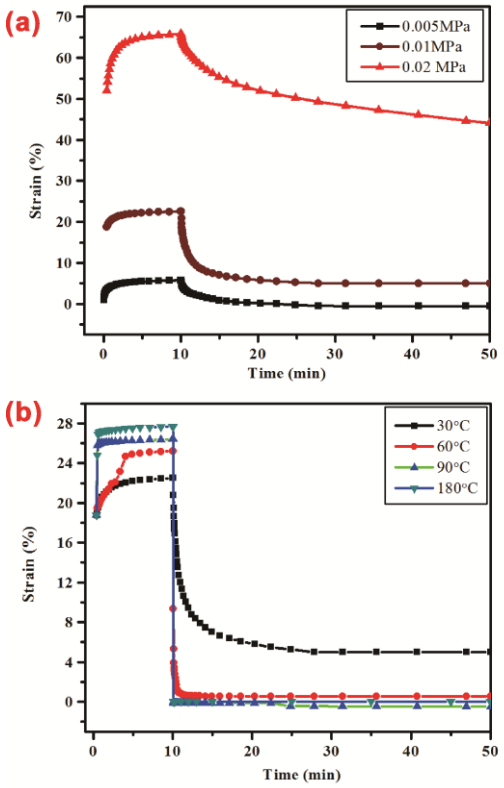

Figure 3. (a) Creep curves of BNNS aerogel-20 at different stress magnitudes. (b) Temperature dependence of creep recovery curves of BNNS aerogel-20 at 0.01 MPa.

Furthermore, the generalized Voigt-Kelvin model,[35] was used to simulate the creep behavior of the BNNS aerogel-20, as shown in Figure 4a. According to the model, the total strain as a function of time is the sum of the strains resulting from three essentially separate Voigt-Kelvin elements, which are made up of linear spring and linear viscous dashpot. The relationship between stress and strain in the linear spring can be defined by:

$$\sigma_s = E\,\varepsilon_s \quad (1)$$

where σ is the applied stress, E is the spring modulus and ε_s is the strain.

For the linear viscous dashpot, the relationship between stress and strain can be defined by:

$$\sigma_d = \eta \frac{d\varepsilon_d}{dt} \quad (2)$$

where η is the viscosity coefficient of the fluid in the dashpot and $(d\varepsilon_d/dt)$ is the strain rate.

In a Voigt-Kelvin element, the total stress is the sum of the individual stress, while the strain is the same since they are connected in parallel.

$$\sigma_{total} = E\,\varepsilon_s + \eta \frac{d\varepsilon_d}{dt} \quad (3)$$

During the creep process, $\sigma_{total} = \sigma_0$, then Eq. 3 can be translated to:

$$\frac{d\varepsilon}{\sigma_0 - E\,\varepsilon} = \frac{dt}{\eta} \quad (4)$$

When t=0, ε=0, integrating Eq. (4) results in

$$\varepsilon(t) = \varepsilon_\infty - \varepsilon_\infty e^{-\frac{t}{\tau}} \quad (5)$$

Physical Chemistry Chemical Physics Accepted Manuscript

where ε_∞ and τ *(η/E)* are the strain at the equilibrium and relaxation time constant, respectively.

For three Voigt-Kelvin elements connected in series, the total applied stress is distributed across the elements. The evolution of the strain in this case can be described by:

$$\varepsilon(t) = \varepsilon_\infty - \varepsilon_{\infty,1} e^{-\frac{t}{\tau_1}} - \varepsilon_{\infty,2} e^{-\frac{t}{\tau_2}} - \varepsilon_{\infty,3} e^{-\frac{t}{\tau_3}} \quad (6)$$

where $\varepsilon_\infty = \varepsilon_{\infty,1} + \varepsilon_{\infty,2} + \varepsilon_{\infty,3}$, $\varepsilon_{\infty,1}$, $\varepsilon_{\infty,2}$, and $\varepsilon_{\infty,3}$ are the strains at the different equilibrium; τ_1, τ_2, and τ_3 are the relaxation time constants for different unit, respectively. As shown in Figures 4b and 4c, the creep behaviour of the BNNS aerogel is well simulated by the generalized Voigt-Kelvin model at all stress levels and examined temperatures, with a correlation coefficient, R, greater than 0.99. The relaxation time (τ) (Table S1, ESI) varies as a function of applied stress and examined temperatures, indicating the non-linear viscoelasticity of the BNNS aerogel. In addition, with the increase of the constant stress levels and examined temperatures, a decrease in τ is observed. The decreased τ means easy creep, which well agrees with the experiments.

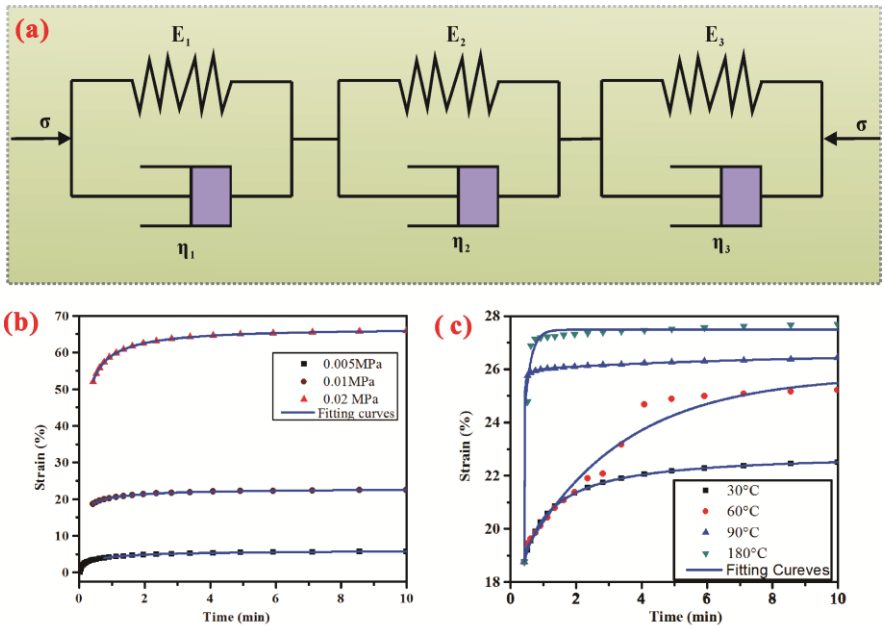

Figure 4. (a) Schematic representation of the generalized Voigt-Kelvin model. (b) and (c): Modeling results of creep of BNNS aerogel at different stress levels (b), and examined temperature (c).

In order to further understand unrecoverable creep deformation, the Weibull-distribution equation was fitted to the recovery data. After removing the applied load, the time-dependent recovery stain, $\varepsilon(t)$, obeys the following equation.[36]

$$\varepsilon(t) = \varepsilon_\upsilon \left[\exp\left(-\left(\frac{t-t_0}{\eta_\tau}\right)^{\beta_\tau}\right)\right] + \varepsilon_\infty \quad (7)$$

where ε_υ is the viscoelastic strain recovery determined by the two parameters including characteristic lift (η_τ) and shape (β_τ) over recovery time t. The parameter t_0 is the time when the applied stress is removed, and ε_∞ is the permanent strain from viscous flow effects.

Figure 5 shows the fitting results of the experimental curves of the recovery strain as a function of time. The various parameter values were obtained (Table S2, ESI). The results indicate that Weibull-Distribution equation provides a good representation of the behaviour of the viscoelastic strain recovery. It is obviously observed that η_τ and ε_∞ increase with the increased stress levels, indicating that the high stress leads to the poor strain recovery which agrees with experiment. In addition, the above-mentioned parameters decrease with temperature, which suggests that BNNS aerogel has high recovery ability at high temperature.

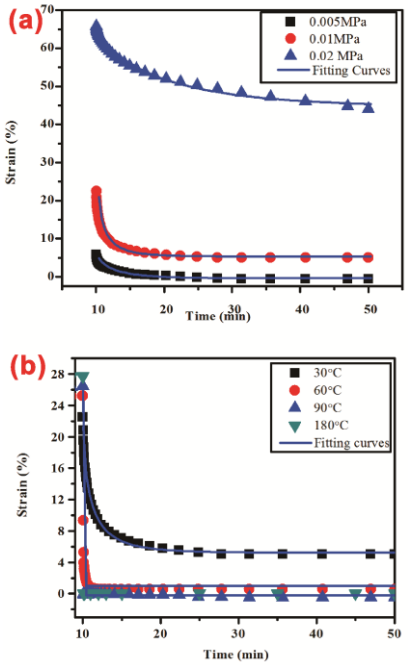

Figure 5. Simulated results of recovery of BNNS aerogel-20 at (a) different stress levels and (b) examined temperature.

Physical Chemistry Chemical Physics Accepted Manuscript

This journal is © The Royal Society of Chemistry 20xx

Please do not adjust margins

Conclusions

The viscoelasticity of boron nitride nanosheet (BNNS) aerogel, including dynamic viscoelasticity and creep behaviour have been investigated at different stress levels and temperature. Classical viscoelastic models, including Voigt-Kelvin model, and Weibull-distribution model were used to simulate the viscoelastic features of BNNS aerogel. The dynamic viscoelasticity study shows that the BNNS aerogel has high damping ratio (0.2), while it manifests lightweight and negligible temperature dependence in the temperature range from 30 to 180 °C. This indicates its potential in vibration damping and acoustic suppression in a variety of dynamic systems. The excellent simulation of creep behaviour by the classical models for BNNS aerogel indicates that the creep origin may result from the intrinsical viscoelasticity of polymer in the aerogel and interfacial sliding at the BNNS-polymer interface. The viscoelasticity found in the aerogel promises its applications as damping materials.

This work is supported by Guangdong and Shenzhen Innovative Research Team Program (No. 2011D052 and KYPT20121228160843692), Shenzhen Electronic Packaging Materials Engineering Laboratory (No.2012-372). J. B. Xu would like to thank the National Science Foundation of China for the support, particularly, via Grant No 61229401.

Notes and references

1. Y. Si, J. Yu, X. Tang, J. Ge and B. Ding, *Nature Commun.*, 2014, **5**, 5802.
2. B. Wicklein, A. Kocjan, G. Salazar-Alvarez, F. Carosio, G. Camino, M. Antonietti and L. Bergstrom, *Nature Nanotech.*, 2015, **10**, 277-283.
3. S. Bullita, A. Casu, M. F. Casula, G. Concas, F. Congiu, A. Corrias, A. Falqui, D. Loche and C. Marras, *PCCP*, 2014, **16**, 4843-4852.
4. Z.-Y. Wu, C. Li, H.-W. Liang, J.-F. Chen and S.-H. Yu, *Angew. Chem. Int. Ed.*, 2013, **52**, 2925-2929.
5. V. Chabot, D. Higgins, A. Yu, X. Xiao, Z. Chen and J. Zhang, *Energy Environ. Sci.*, 2014, **7**, 1564-1596.
6. S. Nardecchia, D. Carriazo, M. Luisa Ferrer, M. C. Gutierrez and F. del Monte, *Chem. Soc. Rev.*, 2013, **42**, 794-830.
7. C. Li and G. Shi, *Adv. Mater.*, 2014, **26**, 3992-4012.
8. Q. Chen, Y. Hu, C. Hu, H. Cheng, Z. Zhang, H. Shao and L. Qu, *PCCP*, 2014, **16**, 19307-19313.
9. J.-S. Lee, H.-J. Ahn, J.-C. Yoon and J.-H. Jang, *PCCP*, 2012, **14**, 7938-7943.
10. L. Song, Q. Luo, F. Zhao, Y. Li, H. Lin, L. Qu and Z. Zhang, *PCCP*, 2014, **16**, 21820-21826.
11. R. Bari, D. Parviz, F. Khabaz, C. D. Klaassen, S. D. Metzler, M. J. Hansen, R. Khare and M. J. Green, *PCCP*, 2015, **17**, 9383-9393.
12. L. H. Li, J. Cervenka, K. Watanabe, T. Taniguchi and Y. Chen, *Acs Nano*, 2014, **8**, 1457-1462.
13. L. H. Li, T. Xing, Y. Chen and R. Jones, *Advanced Materials Interfaces*, 2014, **1**, 1300132.
14. A. Pakdel, C. Zhi, Y. Bando and D. Golberg, *Mater. Today*, 2012, **15**, 256-265.
15. D. Golberg, Y. Bando, Y. Huang, T. Terao, M. Mitome, C. Tang and C. Zhi, *Acs Nano*, 2010, **4**, 2979-2993.
16. A. Pakdel, Y. Bando and D. Golberg, *Chem. Soc. Rev.*, 2014, **43**, 934-959.
17. Y. Zhao, X. Wu, J. Yang and X. C. Zeng, *PCCP*, 2012, **14**, 5545-5550.
18. Q. Cai, L. H. Li, Y. Yu, Y. Liu, S. Huang, Y. Chen, K. Watanabe and T. Taniguchi, *PCCP*, 2015, **17**, 7761-7766.
19. L. Liu, T.-K. Sham and W. Han, *PCCP*, 2013, **15**, 6929-6934.
20. C. Zhi, Y. Bando, C. Tang, H. Kuwahara and D. Golberg, *Adv. Mater.*, 2009, **21**, 2889-2893.
21. X. Wang, C. Zhi, L. Li, H. Zeng, C. Li, M. Mitome, D. Golberg and Y. Bando, *Adv. Mater.*, 2011, **23**, 4072-4076.
22. M. Xu, D. N. Futaba, M. Yumura and K. Hata, *Nano Letters*, 2011, **11**, 3279-3284.
23. W. Knoben, N. A. M. Besseling, L. Bouteiller and M. A. Cohen Stuart, *PCCP*, 2005, **7**, 2390-2398.
24. S. B. Hutchens, A. Needleman and J. R. Greer, *J Mech. Phys. Solids*, 2011, **59**, 2227-2237.
25. J. Suhr, N. Koratkar, P. Keblinski and P. Ajayan, *Nature Mater.*, 2005, **4**, 134-137.
26. M. Xu, D. N. Futaba, T. Yamada, M. Yumura and K. Hata, *Science*, 2010, **330**, 1364-1368.
27. M. Xu, D. N. Futaba, M. Yumura and K. Hata, *Adv. Mater.*, 2011, **23**, 3686-3691.
28. J. Yin, X. Li, J. Zhou and W. Guo, *Nano Letters*, 2013, **13**, 3232-3236.
29. X. Zeng, L. Ye, S. Yu, H. Li, R. Sun, J. Xu and C.-P. Wong, *Nanoscale*, 2015, **7**, 6774-6781.
30. C. Y. Zhi, Y. Bando, C. C. Tang, R. G. Xie, T. Sekiguchi and D. Golberg, *J. Am. Chem. Soc.*, 2005, **127**, 15996-15997.
31. M. H. Malakooti, H.-S. Hwang and H. A. Sodano, *ACS Applied Materials & Interfaces*, 2014, **7**, 332-339.
32. Y. Zeng, L. Ci, B. J. Carey, R. Vajtai and P. M. Ajayan, *Acs Nano*, 2010, **4**, 6798-6804.
33. Z. Gong, J. Gong, X. Yan, S. Gao and B. Wang, *J. Phys. Chem. C*, 2011, **115**, 18468-18472.
34. Y. Chen, D. Yao, H. Zou and M. Liang, *RSC Adv.*, 2014, **4**, 44750-44756.
35. W. N. Findley, J. S. Lai, and K Onaran ed., *creep and relaxation of nonlinear viscoelastic materials*, North-Holland Publishing Company, New York, 1976, Ch. 5 pp. 55-69.
36. X. Wang, L.-X. Gong, L.-C. Tang, K. Peng, Y.-B. Pei, L. Zhao, L.-B. Wu and J.-X. Jiang, *Composites Part A: Applied Science and Manufacturing*, 2015, **69**, 288-298.

Physical Chemistry Chemical Physics Accepted Manuscript

Please do not adjust margins